Available online at www.sciencedirect.com

SciVerse ScienceDirect

Magnetic Resonance Imaging 29 (2011) 1267–1287

MAGNETIC RESONANCE IMAGING

A statistical examination of SENSE image reconstruction via an isomorphism representation

Iain P. Bruce [a], M. Muge Karaman [a], Daniel B. Rowe [a, b,*]

[a] Department of Mathematics, Statistics, and Computer Science, Marquette University, Milwaukee, WI 53201, USA
[b] Department of Biophysics, Medical College of Wisconsin, Milwaukee, WI 53226, USA

Received 4 April 2011; revised 31 May 2011; accepted 6 July 2011

Abstract

In magnetic resonance imaging, the parallel acquisition of subsampled spatial frequencies from an array of multiple receiver coils has become a common means of reducing data acquisition time. SENSitivity Encoding (SENSE) is a popular parallel image reconstruction model that uses a complex-valued least squares estimation process to unfold aliased images. In this article, the linear mathematical framework derived in Rowe et al. [*J Neurosci Meth* 159 (2007) 361–369] is built upon to perform image reconstruction with subsampled data acquired from multiple receiver coils, where the SENSE model is represented as a real-valued isomorphism. A statistical analysis is performed of the various image reconstruction operators utilized in the SENSE model, with an emphasis placed on the effects of each operator on voxel means, variances and correlations. It is shown that, despite the attractiveness of models that unfold the aliased images from subsampled data, there is an artificial correlation induced between reconstructed voxels from the different folds of aliased images. As such, the mathematical framework outlined in this manuscript could be further developed to provide a means of accounting for this unavoidable correlation induced by image reconstruction operators.

Keywords: MRI; fMRI; SENSE; Parallel imaging; Sub-sampled data; Aliasing; Coil covariance; Induced operator correlation

1. Introduction

The discovery that the spatial information of an object can be encoded in the resonance spectrum by a magnetic field gradient [1,2] is the fundamental basis for image formation in magnetic resonance imaging (MRI). Although several mathematical basis sets (Fourier, Hadamard, Wavelet, singular value decomposition) have been used to encode the spatial information of an object, Fourier encoding is by far the most prevalent. The complex-valued spatial frequencies of a real-valued object, Fourier encoded by magnetic field gradients, are not measured instantaneously and thus need to be measured individually in a serial fashion. It can take on the order of 1 to 2 s to measure the required spatial frequencies to form a volume of images at resolutions as low as 64×64 voxels with up to 10 slices. As such, significant effort has been put forth on many fronts, including the measurement of spatial frequencies with multiple receiver coils, in parallel, to decrease image acquisition time [3].

A variety of parallel acquisition methods, such as SENSitivity Encoding (SENSE), use multiple receiver coils to subsample spatial frequency points in parallel and later combine the multiple coil images into a single image [4]. SENSE is a popular parallel image reconstruction technique as it is very flexible in terms of the choice of coil layout, and the reduction in scan time achieved by subsampling the data relaxes the requirements placed on studies such as breath holding in cardiac imaging [5]. Although subsampling data in parallel can dramatically reduce the time involved in acquiring data, it conversely results in an increase in image reconstruction time and difficulty.

SENSE utilizes a linear regression method based on a complex-valued regression coefficient estimation process with transposes replaced by Hermitians to obtain complex-valued images. An unavoidable consequence of the SENSE model that, to the best of our knowledge, has not been discussed is that the "unfolding" process involved in generating a full field-of-view (FOV) image from subsampled data induces a

* Corresponding author.
E-mail address: daniel.rowe@marquette.edu (D.B. Rowe).

0730-725X/$ – see front matter © 2011 Elsevier Inc. All rights reserved.
doi:10.1016/j.mri.2011.07.016

correlation between the aliased voxels from each "fold." This correlation can in turn be amplified if preprocessing operators such as image smoothing are utilized, resulting in regions of voxels correlated with the corresponding regions from other folds. The correlations induced in the real, imaginary, and between real and imaginary components of the data cannot be observed if the operation is carried out on a voxel-by-voxel basis using complex-valued operators, making the use of a real-valued isomorphism invaluable. As this correlation is set in place before any analysis has been performed on the image itself, it is obvious that any correlations deduced from the data could be very misleading after image reconstruction. Attempts to model the induced correlation after image reconstruction (and magnitude-only image formation) would also be extremely challenging.

In this article, we utilize the mathematical framework derived in Ref. [6] to represent the operators involved in image reconstruction in a linear matrix-multiplication fashion. The AMMUST (A Mathematical Model for Understanding the STatistical effects) framework for analyzing reconstruction and preprocessing operators described in Ref. [7] is expanded upon to allow for subsampled data from multiple receiver coils to be used in the SENSE reconstruction model. The operators involved in SENSE image reconstruction are used to illustrate the correlation induced between the aliased voxels of subsampled data, as well as the amplification of said correlation when preprocessing operations such as image smoothing are applied. The correlations induced by the SENSE operators are theoretically illustrated on 96×96 noiseless phantom data as well as on experimental phantom and human subject functional MRI (fMRI) data. A real-valued isomorphism representation of the complex-valued coil covariance matrix is estimated from an experimental time series of scans of a spherical phantom and an experimental time series of nontask scans with a human subject.

2. Theory

2.1. Image reconstruction operators

The AMMUST framework in Ref. [7] generalized the mathematical formalism of image reconstruction in Ref. [6] using a Cartesian linear image reconstruction. The current work expands upon this Cartesian framework in a manner that accounts for the acquisition of subsampled data from an array of receiver coils. This allows for the examination of statistical properties of parallel image reconstruction.

The ability to perform a complex-valued inverse Fourier reconstruction by means of a real-valued isomorphism, a real-valued process for performing a complex-valued operation, as derived in Ref. [6], paves the way for a statistical analysis of the operations commonly undertaken by parallel data acquisition and reconstruction techniques such as SENSE. The real-valued isomorphism allows a reconstructed complex-valued image, in vector form, y, to be represented as the product of an inverse Fourier reconstruction operator, Ω, with the observed complex-valued k-space spatial frequencies in vector form, f, as:

$$y = \Omega f. \tag{1}$$

It can be shown that the above equation holds true for any linear reconstruction operator, Ω; however, the inverse Fourier transform is utilized throughout the remainder of this study. If F_C is a $p_y \times p_x$ matrix of two-dimensional complex-valued spatial frequencies, composed of the sum of a true noiseless complex-valued spatial frequency matrix F_{0C} and a matrix of complex-valued measurement error E_C,

$$F_C = F_{0C} + E_C, \tag{2}$$

then the vector of observed k-space spatial frequencies, f, in Eq. (1) is formed by stacking the $p_x p_y$ real spatial frequencies on top of the $p_x p_y$ imaginary spatial frequencies

$$f = \mathrm{vec}\left(Re\left(F_C^T\right), Im\left(F_C^T\right)\right),$$

where vec(·) is a vectorization operator that stacks the columns of its matrix argument, Re denotes the real part and Im denotes the imaginary part. This vectorization thus concatenates the rows of the real and imaginary matrices into separate vectors, which are in turn concatenated into a single vector, f, that is of dimension $2p_x p_y \times 1$. As with F_C, f is the sum of a vector of true noiseless (complex-valued) spatial frequencies, f_0, and a vector of (complex-valued) measurement error, ε. Similarly to the observed k-space data, if the complex-valued reconstructed image is of dimensions $p_y \times p_x$, then the reconstructed image vector will consist of $p_x p_y$ real reconstructed image values stacked above $p_x p_y$ imaginary reconstructed image values, resulting in a reconstructed image vector y of dimensions $2p_x p_y \times 1$.

Given that the complex-valued reconstructed magnetic resonance image is an inverse Fourier transform (IFT) of the measured complex-valued spatial frequencies,

$$Y\left(q_x \Delta x, q_y \Delta y\right) = \sum_{q_y=-m}^{m-1} \sum_{q_x=-n}^{n-1} F\left(p_x \Delta x, p_y \Delta y\right) exp\left(i2\pi\left(\frac{p_x q_x}{2n} + \frac{p_y q_y}{2m}\right)\right)$$

consider the inverse Fourier transform matrices in the x and y directions

$$\Omega_{xC} = \Omega_{xR} + i\Omega_{xI}, \quad \Omega_{yC} = \Omega_{yR} + i\Omega_{yI}$$

where Ω_{xR} and Ω_{xI} denote the real and imaginary matrix parts, respectively, in the x direction [6]. The jkth element of Ω_{xC} can be expressed as

$$\left(\Omega_{xC}\right)_{jk} = exp\left(\frac{i2\pi}{p_x} + \left(j - \left(\frac{p_x}{2} + 1\right)\right) * \left(k - \left(\frac{p_x}{2} + 1\right)\right)\right),$$

where j and k vary from 1 to p_x [7]. A similar inverse Fourier matrix can be expressed for Ω_{yC} that is of dimension p_y.

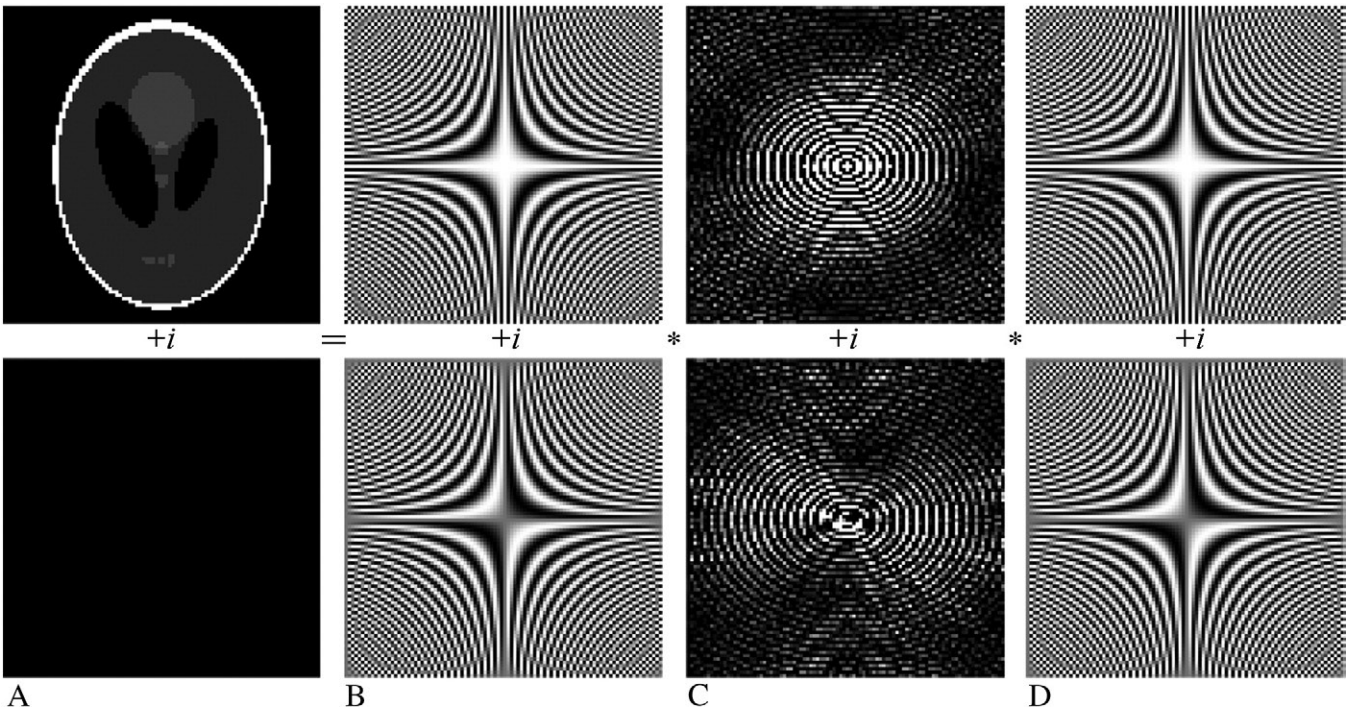

Fig. 1. Inverse Fourier transform of complex spatial frequencies. (A) Reconstructed image Y_C. (B) Ω_{yC} inverse Fourier transform matrices. (C) Spatial frequencies F_C. (D) Ω_{xC} inverse Fourier transform matrices.

Both Ω_{xC} and Ω_{yC} can be adjusted to account for intra-acquisition decay and magnetic field inhomogeneities acquired in the k-space signal [7,8] if T_2* or ΔB maps can be obtained. The complex-valued inverse Fourier transformation of F_C can be written as

$$Y_C = \Omega_{yC} F_C \Omega_{xC}. \tag{3}$$

The inverse Fourier transformation of spatial frequencies used in Eq. (3) is illustrated in Fig. 1. Fig. 1A shows the k-space spatial frequency matrix F_C that is premultiplied by the inverse Fourier transform matrix Ω_{yC} in Fig. 1B and postmultiplied by the inverse Fourier transform matrix Ω_{xC} in Fig. 1D, resulting in the complex-valued image space image in Fig. 1A.

For simplicity in representation and examination of reconstruction, it can be shown that the pre- and post-multiplication of inverse Fourier matrices can be combined into a single reconstruction matrix

$$\Omega = \begin{bmatrix} \Omega_R & -\Omega_I \\ \Omega_I & \Omega_R \end{bmatrix}$$

that is, $2p_xp_y \times 2p_xp_y$, where the real and imaginary components are derived using the Kronecker product, $\otimes$, as

$$\Omega_R = \left[\left(\Omega_{yR} \otimes \Omega_{xR}\right) - \left(\Omega_{yI} \otimes \Omega_{xI}\right)\right],$$
$$\Omega_I = \left[\left(\Omega_{yR} \otimes \Omega_{xI}\right) + \left(\Omega_{yI} \otimes \Omega_{xR}\right)\right].$$

The Kronecker product operator multiplies every element of its first matrix argument by its entire second matrix argument. Premultiplying the spatial frequency vector, f, by the combined inverse Fourier transform matrix, Ω, the reconstructed image in Eq. (1) can be expressed as

$$\begin{pmatrix} y_R \\ y_I \end{pmatrix} = \begin{bmatrix} \Omega_R & -\Omega_I \\ \Omega_I & \Omega_R \end{bmatrix} \begin{pmatrix} f_{0R} + \varepsilon_R \\ f_{0I} + \varepsilon_I \end{pmatrix}. \tag{4}$$

While the spatial frequency vector, f, may be composed of real and imaginary values, the application of the Fourier transform operator in Eq. (4) results in a covariance between the real measurements, a covariance between the imaginary measurements, and a covariance between the real and imaginary (real/imaginary). Eq. (4) lays the groundwork for the AMMUST framework in Ref. [7] that is necessary to analyze the operations involved in image reconstruction for fully sampled data from a single receiver coil. With mere inverse Fourier image reconstruction, the covariance matrix of the reconstructed image is modified by the reconstruction operator Ω as

$$cov(y) = \Omega \Gamma \Omega^T, \tag{5}$$

where Γ is the covariance matrix of the observed vector of k-space data. It is important to note that, although Γ might only have a real and imaginary covariance structure, the resultant covariance in Eq. (5) will also have a covariance between the real and imaginary as well as a covariance between the imaginary and real (imaginary/real). With additional operators to be described later, such as permutations, image smoothing and

the SENSE unfolding operator, the reconstruction in Eq. (1) becomes

$$y = Of, \tag{6}$$

where O signifies the series of linear operators expressed as matrix multiplications applied throughout the image reconstruction process. Just as in Eq. (5), the covariance matrix induced through a series of operators, O, can be calculated by

$$\Sigma = cov(y) = O\Gamma O^{\mathrm{T}}. \tag{7}$$

Similar to the structure of the spatial frequencies in Eq. (2), Γ is the covariance of the spatial frequencies, f, which is composed of a mean signal vector, f_0, and a noise vector, ε. The covariance matrices Γ and Σ contain real-by-real, imaginary-by-imaginary and real-by-imaginary covariances. The vectors f_0 and ε contain real and imaginary spatial frequencies and noise elements. The derivation outlined in the Appendices of Ref. [7] allows for the covariance structure of the square of the magnitude-only data (magnitude-squared data) to be derived from the covariance matrix Σ in Eq. (7) assuming normality. Magnitude-squared data are considered in the analysis of the covariance and correlation induced by operators involved in image reconstruction because an analytical solution exists for the linear framework in this study, while magnitude-only data are not considered as magnitude operations and are not linear in nature. It can be shown that the correlation of magnitude-squared data is asymptotically equivalent to the correlation of magnitude-only data and thus will be used along with complex-valued data to observe properties of real, imaginary and real/imaginary correlation structures.

2.2. Parallel imaging of subsampled data

Although Eq. (4) is expressed for data from a single receiver coil that acquires a full FOV, it can be generalized to reconstruct subsampled data from an array of multiple receiver coils. Traditionally, undersampling data occurs by skipping lines of k-space in the phase encoding (PE) direction, although the framework and principle can be applied for any direction, with any scheme in which lines of data are subsampled. In this Cartesian framework, the subscript y denotes the PE direction (i.e., top–bottom), while the subscript x denotes the frequency encode direction (i.e., left–right). For an acceleration factor (also commonly known as a reduction factor), A, a receiver coil would only acquire every Ath line of k-space in the PE direction. Thus, a subsampled matrix of spatial frequencies F_{C} would be of dimension $(p_y/A)\times p_x$. This subsampled data set is vectorized in exactly the same fashion as the full data set in Eq. (2), where the vector of observed subsampled k-space spatial frequencies, f, in Eq. (1) is formed by stacking the $p_x(p_y/A)$ real spatial frequencies on top of the $p_x(p_y/A)$ imaginary spatial frequencies. In order to utilize the inverse Fourier reconstruction operator, Ω, it is necessary for $\Omega_{y\mathrm{C}}$ to include the correct dimension to transform the reduced FOV.

As will be illustrated, when implementing a SENSE image reconstruction of subsampled data from multiple receiver coils, it is necessary to select an acceleration factor that is less than the total number of coils in the array; otherwise, it results in a sensitivity matrix that is not sufficiently defined. As such, in order to implement the process of subsampling data with an acceleration factor greater than A=1, it is necessary to have more than one receiver coil.

Consider an array of N_{C} receiver coils, each of which acquires a $(p_y/A)\times p_x$ subsampled spatial frequency matrix. The vector of spatial frequencies, f, will be composed of N_{C} vectors of the vectorized real spatial frequencies from each coil stacked above the imaginary component of spatial frequencies from the corresponding coils. In this form, the vectorized spatial frequencies from each coil can be inverse Fourier transformed via the Ω operator, as in Eq. (4), by carrying out the Kronecker product $I_{\mathrm{N_C}}\otimes\Omega$.

In this Kronecker product, every element of $I_{\mathrm{N_C}}$ is multiplied by the entire matrix Ω, generating a block diagonal inverse Fourier reconstruction operator for a reduced FOV image reconstruction of each coil image

$$y_{\mathrm{coil}} = (I_{N_{\mathrm{C}}} \otimes \Omega)f, \tag{8}$$

where

$$y_{\mathrm{coil}} = \mathrm{vec}\left(Re\left(y_{\mathrm{coil}}^{\mathrm{T}}\right), Im\left(y_{\mathrm{coil}}^{\mathrm{T}}\right)\right)$$

is a vector concatenating the subvectors coil=[1, 2,…, N_{C}] of the real reconstructed coil images stacked upon the corresponding imaginary reconstructed coil images. The consequence of skipping lines in k-space is an aliased image. This effect is illustrated in Fig. 2 where a magnitude image of a modified Shepp–Logan phantom (top left) represented by its spatial frequencies (top right) is reduced by a factor of A=3 (bottom right) in the PE direction (top–bottom) to produce an aliased image (bottom left).

The aliased images from the N_{C} receiver coils are combined and unaliased, or "unfolded," via the SENSE unfolding matrix in conjunction with the coil covariance matrix. The combination of these images first requires a permutation that rearranges the vector y_{coil}, which was ordered by coil image, to now being ordered by voxel. The result of such a permutation is another vector containing the same elements, but the elements are rearranged with the N_{C} real image values stacked upon N_{C} imaginary image values for each aliased voxel in the N_{C} coil images. This reordering operation can be undertaken by premultiplying the product $(I_{\mathrm{N_C}}\otimes\Omega)f$ by a complex permutation matrix P_{C}, resulting in a vector of elements ordered by reduced FOV folded image space voxel values

$$a = P_{\mathrm{C}}(I_{N_{\mathrm{C}}} \otimes \Omega)f. \tag{9}$$

A permutation matrix such as P_{C} is a matrix of zeros and ones that when premultiplying a vector, the resulting vector contains the same elements but in a different order. In addition to the complex permutation applied in Eq. (9), for

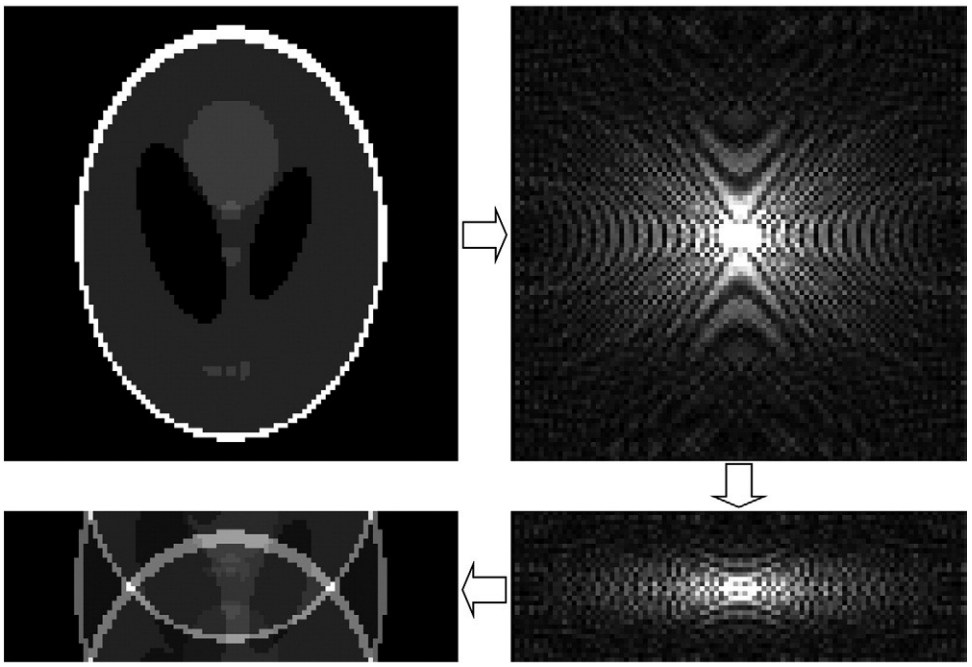

Fig. 2. Image aliasing resulting from subsampled *k*-space.

even acceleration factors, it may be necessary to apply a second permutation that performs a Fourier transform shift. For an acceleration factor of A=2, the center line of *k*-space will be in the center of the aliased image, and thus an "unfolding" will lead to an image that does not fulfill the Nyquist criteria. This ultimately results in the reconstructed image in Fig. 3A that appears to be off center. However, if a Fourier transform shift is applied to the aliased images after Fourier reconstruction, then the center line of *k*-space will align itself with the edge of a fold. Consequently, the folds themselves will align their edges with the edge of the full FOV, as illustrated in Fig. 3B. This is not, however, an issue for odd acceleration factors, as illustrated in Fig. 3C for an acceleration factor of A=3. This is because, although the center line of *k*-space lies within the center of a fold, when unfolding the aliased images, the edges of the folds are aligned with the edge of the full FOV as well. As such, a Fourier transform shift permutation, P_S, premultiplies the complex permutation in Eq. (9) whenever an even acceleration factor, A, is selected

$$a = P_S P_C (I_{N_C} \otimes \Omega) f. \tag{10}$$

2.3. SENSE

Within the SENSE model with N_C receiver coils, voxel j contains a complex-valued vector $a_{jC}=a_{jR}+i\,a_{jI}$ of N_C voxel measurements from the subsampled spatial frequencies, which are derived by

$$a_{jC} = S_{jC} v_{jC} + \varepsilon_{jC}. \tag{11}$$

In Eq. (11), $S_{jC}=S_{jR}+iS_{jI}$ is derived from the fully sampled complex-valued coil image sensitivity matrix, $v_{jC}=v_{jR}+iv_{jI}$ is the complex-valued true scalar voxel and $\varepsilon_{jC}=\varepsilon_{jR}+i\varepsilon_{jI}$ is the complex-valued additive measurement noise. For the estimation

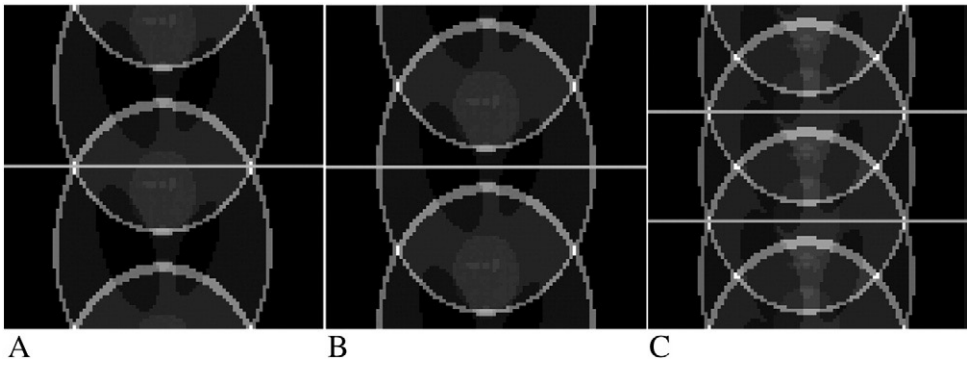

Fig. 3. Fourier transform shift permutation required for even acceleration factors. (A) A=2 inverse Fourier transform (IFT) without shift. (B) A=2 IFT with shift. (C) A=3 IFT without shift.

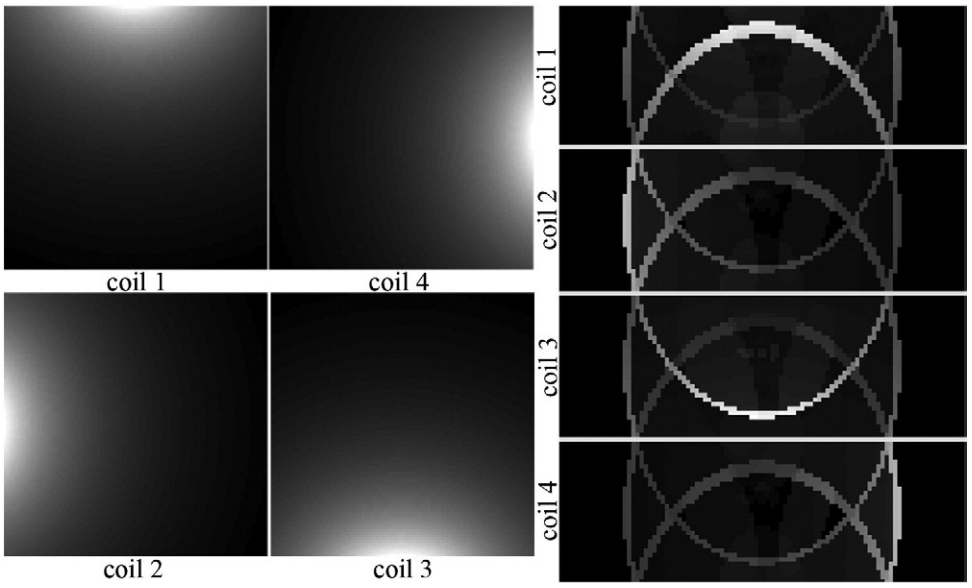

Fig. 4. Sensitivity maps and their corresponding aliased coil images for an array of N_C=4 coils.

of each of the aliased voxel values, the matrix S_{jC} is of dimension $N_C \times A$, a_{jC} and ε_{jC} are of dimension $N_C \times 1$, while v_{jC} is a vector of length A denoting values of each of the A aliased voxel values. It is generally assumed that the complex-valued measurement noise, ε_{jC}, is derived from the complex-valued normal distribution [9] given by

$$f(\varepsilon_{jC}) = (2\pi)^{-N_C} |\Psi_C|^{-1/2} exp\left(-\frac{1}{2}\varepsilon_{jC}^H \Psi_C^{-1} \varepsilon_{jC}\right),$$

where $\Psi_C = \Psi_R + i\Psi_I$ is the complex-valued coil covariance matrix and H denotes the Hermetian or conjugate transpose. With this error structure, the complex-valued vector of subsampled spatial frequencies, a_{jC}, can be shown with a change of variables to have a complex-valued normal distribution

$$f(a_{jC}) = (2\pi)^{-N_C} |\Psi_C|^{-1/2} \times exp\left[-\frac{1}{2}(a_{jC} - S_{jC}v_{jC})^H \Psi_C^{-1}(a_{jC} - S_{jC}v_{jC})\right]. \quad (12)$$

The least squares estimate of the complex-valued true scalar voxel values, as used for the SENSE estimate of the unaliased single combined voxel values, is

$$v_{jC} = \left(S_{jC}^H \Psi_C^{-1} S_{jC}\right)^{-1} S_{jC}^H \Psi_C^{-1} a_{jC}. \quad (13)$$

Alternatively, Eq. (11) can be expressed as a real-valued isomorphism

$$a_j = S_j v_j + \varepsilon_j, \quad (14)$$

where $a_j = (a_{jR}^T, a_{jI}^T)^T$ is a vector of N_C real measurements stacked upon a vector of N_C imaginary measurements and $\varepsilon_j = (\varepsilon_{jR}^T, \varepsilon_{jI}^T)^T$ is a vector of the N_C real parts of the complex-valued additive noise stacked upon a vector of the N_C imaginary parts. The vector of the complex-valued scalar voxel values $v_j = (v_{jR}^T, v_{jI}^T)^T$ is also composed of the real part stacked upon the imaginary part. The unfolded scalar voxel values, v, are derived from an array of fully sampled spatial frequencies from each coil

$$S_j = \begin{bmatrix} S_{jR} & -S_{jI} \\ S_{jI} & S_{jR} \end{bmatrix}, \quad (15)$$

where S_{jR} and S_{jI} are the real and imaginary matrices of coil image sensitivities for the voxel of interest j in the folded image. The aliased surface coil images, from the reception field sensitivities of the N_C=4 receiver coils in Fig. 4A, are illustrated in Fig. 4B.

With the use of the isomorphism in Eq. (14), the complex-valued multivariate normal distribution can be expressed as the $2N_C \times 1$ multivariate normal distribution of coil measurements in Eq. (12) by

$$f(a_j) = (2\pi)^{-N_C} |\Psi|^{-1/2} \times exp\left[-\frac{1}{2}(a_j - S_j v_j)^T \Psi^{-1}(a_j - S_j v_j)\right].$$

As the additive measurement noise derived from the complex-valued normal distribution

$$\varepsilon_{jC} \sim CN(0, \Psi_C)$$

provides the correlation between the coils in the SENSE model, when represented as a real-valued isomorphism,

$$\varepsilon_j \sim N\left(0, \begin{bmatrix} \Psi_R & -\Psi_I \\ \Psi_I & \Psi_R \end{bmatrix}\right),$$

the real-valued isomorphism of the complex coil covariance matrix, as used in the SENSE model, is expressed as

$$\Psi = \begin{bmatrix} \Psi_R & -\Psi_I \\ \Psi_I & \Psi_R \end{bmatrix}. \quad (16)$$

What Eq. (16) implies is that the real/imaginary covariance between coils is the negative of the imaginary/real, making the overall coil covariance structure skew-symmetric. In many studies, Ψ_C (and hence Ψ) is treated as a real-valued identity matrix; however, it will be shown in the experimental illustration that this is far from the correct structure when the coil covariance is estimated from real data.

Provided with the real-valued isomorphism representation of the complex-valued coil sensitivities matrix in Eq. (15) and the real-valued isomorphism representation of the complex-valued coil covariance matrix as in Eq. (16), the SENSE estimation of the unaliased single combined voxel values in Eq. (13) can be equivalently expressed as a real-valued isomorphism

$$\begin{bmatrix} v_{j\mathrm{R}} \\ v_{j\mathrm{I}} \end{bmatrix} = \left(\begin{bmatrix} S_{j\mathrm{R}} & -S_{j\mathrm{I}} \\ S_{j\mathrm{I}} & S_{j\mathrm{R}} \end{bmatrix}^{\mathrm{T}} \begin{bmatrix} \Psi_R & -\Psi_I \\ \Psi_I & \Psi_R \end{bmatrix}^{-1} \begin{bmatrix} S_{j\mathrm{R}} & -S_{j\mathrm{I}} \\ S_{j\mathrm{I}} & S_{j\mathrm{R}} \end{bmatrix} \right)^{-1} \times \begin{bmatrix} S_{j\mathrm{R}} & -S_{j\mathrm{I}} \\ S_{j\mathrm{I}} & S_{j\mathrm{R}} \end{bmatrix}^{\mathrm{T}} \begin{bmatrix} \Psi_R & -\Psi_I \\ \Psi_I & \Psi_R \end{bmatrix}^{-1} \begin{bmatrix} a_{j\mathrm{R}} \\ a_{j\mathrm{I}} \end{bmatrix}$$

or

$$v_j = \left(S_j^{\mathrm{T}} \Psi^{-1} S_j \right)^{-1} S_j^{\mathrm{T}} \Psi^{-1} a_j \quad (17)$$

for each voxel j, where S_j is of dimension $2N_C \times 2A$, Ψ is of dimension $2N_C \times 2N_C$ and the vector of voxel measurements a_j is of dimension $2N_C \times 1$. Thus, the isomorphism in Eq. (17) yields an image space vector, v_j, of dimension $2A \times 1$ that is composed of the A real voxel values stacked upon the A imaginary voxel values. These A values correspond to the A folds that are formed via undersampling the data in k-space by a factor of A. It can be shown that the real and imaginary parts of the estimated complex-valued unaliased single combined image voxel value in Eq. (13) are mathematically equivalent to the estimated real and imaginary isomorphism vector of unaliased single combined image voxel value in Eq. (17).

In order to carry out the SENSE isomorphism using the linear framework in Eqs. (8) to (10), Eq. (17) is rewritten as

$$v = Ua,$$

where the SENSE unfolding matrix U is block diagonal with the jth block unfolding the aliased voxel j

$$U_j = \left(S_j^{\mathrm{T}} \Psi^{-1} S_j \right)^{-1} S_j^{\mathrm{T}} \Psi^{-1}$$

and

$$a = P_S P_C (I_{N_C} \otimes \Omega) f.$$

The SENSE estimation in Eq. (17) can be expressed as a single operator to unfold all aliased voxels in the reduced images at once. Provided with the fully sampled coil sensitivities, S_j, a coil sensitivity matrix, S, can be constructed by placing the $2N_C \times 2A$ coil sensitivities corresponding to each aliased voxel, j, where j varies from voxel 1 to voxel rp, along the diagonal of a block diagonal matrix. With a covariance between voxels of Υ, the covariance structure of the k-space data, acquired from independent receiver coils, with a coil covariance of Ψ is defined to be

$$\Gamma = \frac{p_x p_y}{A} (\Psi \otimes \Upsilon), \quad (18)$$

where $p_x(p_y/A)$ is a scalar multiple produced by the Fourier transformation from image space to k-space. In order to reconstruct all voxels at once with a voxel covariance Υ, the SENSE unfolding operators are expressed as

$$U = \left(S^{\mathrm{T}} (\Upsilon \otimes \Psi)^{-1} S \right) S^{\mathrm{T}} (\Upsilon \otimes \Psi)^{-1}, \quad (19)$$

where the orders of Ψ and Υ in Eq. (18) are switched in the Kronecker product in Eq. (19) because the data being unfolded are ordered by voxel rather than by coil. As the SENSE reconstruction is traditionally carried out on a voxel-by-voxel basis, this necessarily implies that the general practice is to use an identity covariance between voxels in the SENSE model. Therefore, despite the fact that the coil sensitivities may in fact have spatial variability, if Υ is assumed to be an identity matrix with rp diagonal elements, the SENSE unfolding operator is

$$U = \left(S^{\mathrm{T}} (I_{rp} \otimes \Psi)^{-1} S \right) S^{\mathrm{T}} (I_{rp} \otimes \Psi)^{-1}.$$

When U is applied as an operator, it will perform the real-valued estimation in Eq. (17), "unfolding" the N_C real and N_C imaginary voxel values in all rp aliased voxels from the N_C coils into A real and A imaginary voxel values for each of the A folds

$$v = UP_S P_C (I_{N_C} \otimes \Omega) f.$$

It is then necessary to apply a third permutation, P_U, that reorders the unaliased real and imaginary image values in v from being ordered by voxel to being ordered by fold and then from being ordered by fold to being ordered by row, resulting in a vector of all real image values stacked upon all imaginary image values

$$y = P_U U P_S P_C (I_{NC} \otimes \Omega) f \quad (20)$$

or

$$y = P_U v.$$

Additional operators for preprocessing in k-space, O_K, and image space processing, O_I, can be incorporated into Eq. (20) as

$$y = O_I P_U U P_S P_C (I_{N_C} \otimes \Omega O_K) f.$$

These operators are treated as identity in this study unless specified otherwise. The operators used to reconstruct the acquired k-space data in Eq. (20) can be combined into a single operator as

$$O = O_I P_U U P_S P_C (I_{N_C} \otimes \Omega O_K). \quad (21)$$

From this collection of operators, the modified covariance by the reconstruction and preprocessing operators themselves can be evaluated as

$$\Sigma_{SE} = cov(y) = O \Gamma O^T,$$

where Γ is the covariance matrix of the acquired k-space data. In the analysis of the statistical properties induced by the reconstruction operators, Γ is assumed to be identity and thus any Σ that is not proportional to an identity matrix is an induced covariance between voxels. As such, the induced covariance between voxels from the SENSE reconstruction operators is

$$\begin{aligned}\Sigma_{SE} &= OO^T \\ &= O_I P_U U P_S P_C (I_{N_C} \otimes \Omega O_K)(I_{N_C} \otimes \Omega O_K)^T P_S^T P_S^T U^T P_U^T O_I^T.\end{aligned}$$

Thus, for any of the operators in Eq. (21), such as the unfolding permutation P_U, the covariance induced by that operator of choice is evaluated as

$$\Sigma_{P_U} = P_U O_U O_U^T P_U^T$$

where $O_U = U P_S P_C (I_{N_C} \otimes \Omega O_K)$ denotes the collection of all operators premultiplied by P_U in Eq. (21). Therefore, if the operators in O_U are all orthogonal, Σ will be either an identity matrix or a scaled identity matrix.

For an arbitrary operator (or collection of operators) O, assuming spatial frequencies with an identity covariance between voxels, the correlation induced between voxels is derived by

$$\mathrm{corr}(O) = D_O^{-1/2} O O^T D_O^{-1/2}, \quad (22)$$

where $D_O = \mathrm{diag}(\Sigma)$ is a diagonal matrix of the variances from the diagonal of the covariance matrix $\Sigma = OO^T$ and the $-1/2$ superscript denotes that the diagonal elements are square rooted and inverted. The real-valued isomorphism correlation matrix produced by Eq. (22) can be partitioned into quadrants as

$$\mathrm{corr}(\Sigma) = \begin{bmatrix} RR & RI \\ IR & II \end{bmatrix},$$

where any row, j, of each quadrant denotes the correlation between voxel j and all other voxels in the reconstructed image for the respective complex denomination. The correlation about voxel j can be generated by partitioning the jth row of each quadrant in $\mathrm{corr}(\Sigma)$ into p_x vectors of $1 \times p_y$ (each of which denotes a column of the reconstructed image), stacking the row vectors into a matrix and finally transposing.

2.3.1. Selection of the acceleration factor A

It is necessary for N_C to be greater than the acceleration factor A in order to perform the inversion in the complex-valued weighted least squares estimation in the SENSE model [10]. An increase in acceleration factor, A, is marked by a decrease in the number of signal values received by each coil by a factor of A. Transitioning from k-space to image space via inverse Fourier transform, the image-space variance is equivalent to the original k-space variance divided by the k-space dimensions. Thus, a reduction in k-space dimensions, by a factor of A, effectively scales the standard deviation in image space by a factor of $(A)^{1/2}$. Therefore, the ratio between the signal-to-noise ratio (SNR) of a full FOV acquisition and a reduced FOV in a voxel j is expressed as

$$\mathrm{SNR}_j^{red} = \frac{\mathrm{SNR}_j^{full}}{g_j \sqrt{A}},$$

where

$$g_j = \frac{\mathrm{SNR}_j^{full}}{\mathrm{SNR}_j^{red} \sqrt{A}} = \sqrt{\left[\left(S^H \Psi^{-1} S\right)^{-1}\right]_{j,j} \left[\left(S^H \Psi^{-1} S\right)\right]_{j,j}}$$

is the geometry factor (g-factor) and the subscript j,j signifies the diagonal elements of the two terms in the square root. The diagonal elements of the two matrices in brackets above are multiplied then added together. The g-factor is commonly used as a means of assessing the geometry of the array of receiver coils. The g-factor essentially determines the level of noise amplification that results from the reconstruction process and describes how well aliased voxels will be unfolded given the choice of coil geometry. It depends heavily on how different the N_C coil sensitivities are in any aliased voxel j, but is also influenced by the covariance between receiver coils. Ideally, an array of independent receiver coils with sensitivity profiles that do not overlap and do not decrease in strength with distance from the coil (i.e., similar to that of a pie with slices of equal size and constant throughout) would result in a g-factor of 1 in every voxel. However, this coil arrangement is very difficult to achieve, and thus the coil sensitivity profiles usually have considerable overlap. The g-factor is improved by increasing the number of receiver coils and maintaining an acceleration factor, A,

that is somewhat less than N_C [10]. Doing so results in an overdetermined system of equations, improving the numerical condition of the matrix inversion utilized in the SENSE least squares estimation of voxel values in Eq. (17).

3. Theoretical illustration

Within this illustration, data are generated from a true noiseless Shepp–Logan phantom with a theoretical coil covariance consistent with that of real data between N_C=4 receiver coils. Recall from Eq. (6) that a full FOV vectorized image in image space with real image values stacked upon imaginary image values, y, is reconstructed through a variety of operators, O, that premultiply a vector, f, containing a series of N_C subsampled vectors of real k-space data stacked upon corresponding vectors of imaginary k-space data. Starting with a real-valued isomorphism representation of a true noiseless real-valued Shepp–Logan phantom, y, the vector of k-space data, f, can be derived from Eq. (6) with a least squares estimation by

$$f = (O^T O)^{-1} O^T y.$$

Under the assumption that there is an identity covariance structure between voxels in Eq. (19), the result of this procedure is a vector of subsampled k-space data from N_C receiver coils that exhibits an appropriate theoretical covariance between each of the coils, consistent with that of real data.

To illustrate the covariance and correlation induced by the individual operators, operators will be generated to reconstruct a 9×9 image with an acceleration factor of A=3, while a 96×96 modified Shepp–Logan phantom image, scaled to have a maximum value of 50, is used to illustrate the correlation induced by operators on the individual voxels themselves. As complex data are gathered in both real and imaginary channels, an appropriate choice of coil covariance, in terms of a real-valued isomorphism matrix, is

$$\Psi_{\text{coil}} = \begin{bmatrix} \Psi_{RR} & \Psi_{RI} \\ \Psi_{RI}^T & \Psi_{II} \end{bmatrix},$$

where $\Psi_{RR}=\Psi_R$ is the real coil covariance, $\Psi_{II}=\Psi_I$ is the imaginary coil covariance and $\Psi_{RI}=\Psi_{IR}^T$ is the covariance between the real and imaginary channels. In this illustration,

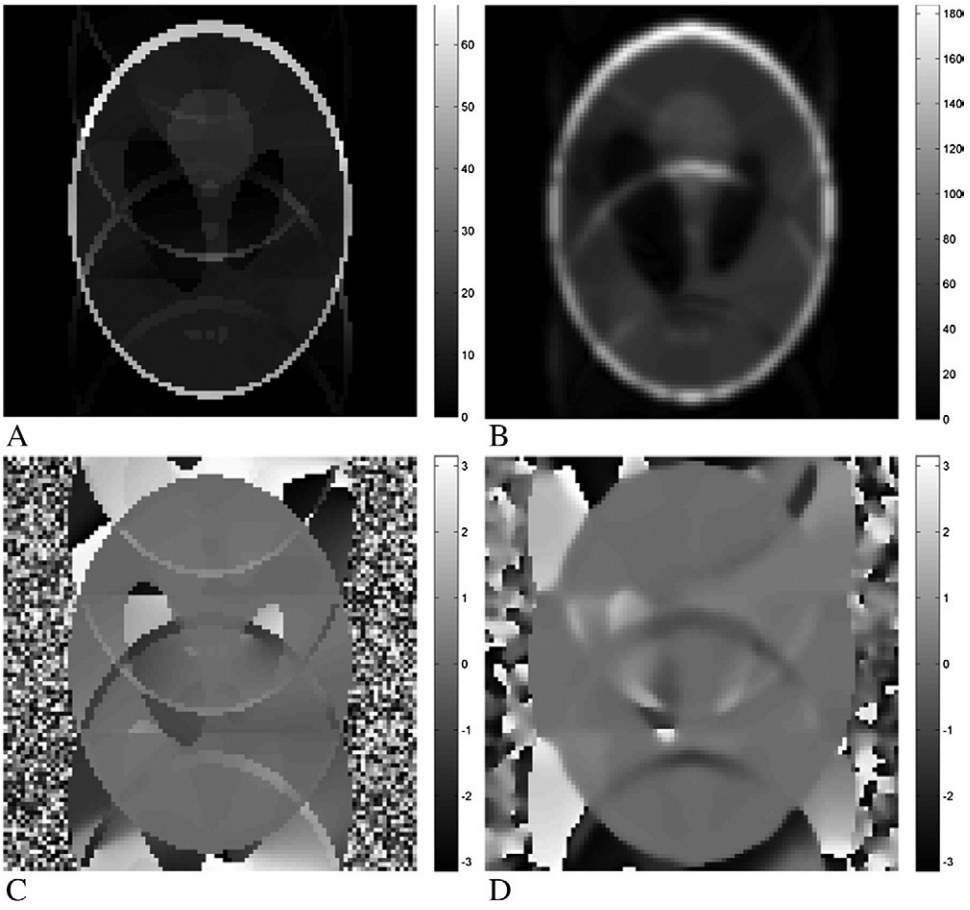

Fig. 5. SENSE magnitude and phase images reconstructed from N_C=4 coils, reduced in the PE direction for an acceleration factor of A=3 with and without smoothing. (A) Unsmoothed magnitude. (B) Unsmoothed phase. (C) Smoothed magnitude. (D) Smoothed phase.

$\Psi_{RI} \neq -\Psi_{IR}^{T}$, making Ψ_{coil} non–skew-symmetric. The real and imaginary coil covariances were chosen to be circular Markovian, resembling the covariance estimated from experimental data as

$$\Psi_R = \Psi_I = \begin{bmatrix} 1 & 0.33 & 0.11 & 0.33 \\ 0.33 & 1 & 0.33 & 0.11 \\ 0.11 & 0.33 & 1 & 0.33 \\ 0.33 & 0.11 & 0.33 & 1 \end{bmatrix}.$$

A nonsymmetric covariance was chosen between the real and imaginary channels to observe the effects of the skew-symmetric coil covariance used in the SENSE model in Eq. (16)

$$\Psi_{RI} = \begin{bmatrix} 0.000 & -0.11 & -0.07 & -0.11 \\ 0.263 & 0.000 & -0.11 & -0.07 \\ 0.417 & 0.263 & 0.000 & -0.11 \\ 0.263 & 0.417 & 0.263 & 0.000 \end{bmatrix}.$$

Reconstructed mean magnitude and phase images are illustrated in Fig. 5. It can be seen in Fig. 5A and C that there appears to be some aliasing in both the magnitude and phase reconstructed images resulting from the skew-symmetric coil

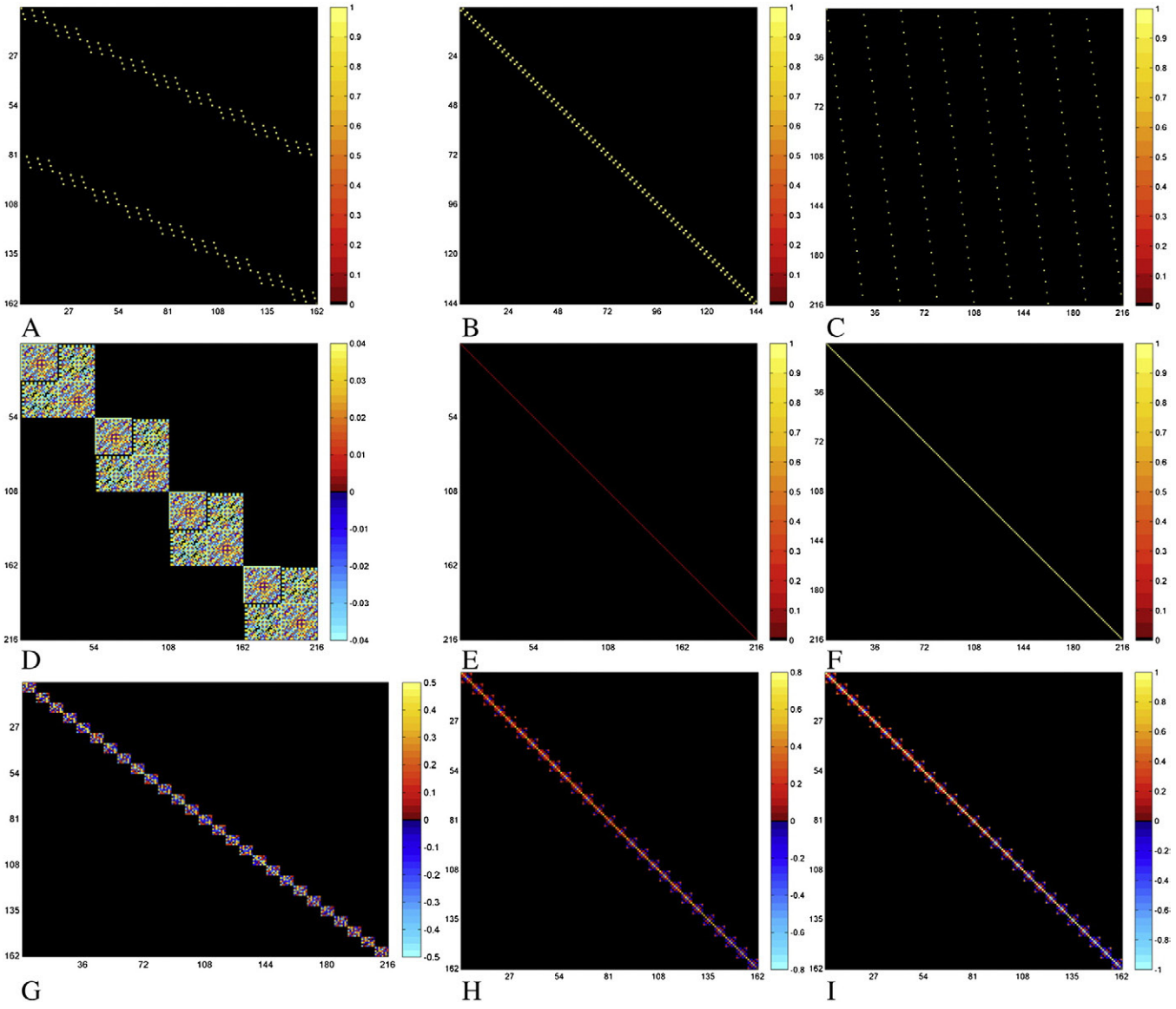

Fig. 6. Operator plots used to reconstruct a 9×9 FOV from N_C=4 coils and an acceleration factor of A=3. (A) Unfolding permutation; (B) shift permutation; (C) complex permutation; (D) inverse Fourier transform operator; (E) covariance induced by the inverse Fourier transform operator; (F) identity correlation induced by the unfolding permutation, shift permutation, complex permutation and inverse Fourier transform operators; (G) SENSE operator; (H) covariance induced by the SENSE operator; (I) correlation induced by the SENSE operator.

covariance structure assumed by the SENSE model in Eq. (16) rather than by the Ψ_{coil} used in generating the data.

As it is common practice to perform image smoothing after reconstruction, a Gaussian kernel, $O_I=S_m$, with a full width at half maximum (FWHM) of three voxels was applied in image space after reconstruction

$$y = S_m P_U U P_S P_C (I_{N_C} \otimes \Omega O_K) f.$$

The SENSE operators for reconstructing k-space data are thus

$$O = S_m P_U U P_S P_C (I_{N_C} \otimes \Omega O_K),$$

where $O_K=I$.

As outlined in Appendix A, in order for the variance of the data to remain unchanged, the magnitude is scaled by the inverse of the square root of the sum of squares of the elements within the Gaussian kernel. For the chosen Gaussian kernel in this illustration, with an FWHM of three voxels, the ratio of the smoothed and unsmoothed mean images is 4.516. One can see this increase in magnitude when comparing the unsmoothed magnitude image in Fig. 5A to those that are smoothed in Fig. 5B. The ghosting in the SENSE magnitude and phase imaged in Fig. 5B and D appears to remain unaffected when the data are smoothed. However, note that the aliasing itself in the SENSE magnitude in Fig. 5A is smoothed and thus becomes spread out to neighboring voxels in Fig. 5B.

Each of the operators in the SENSE model along with the covariance and correlation induced by each operator is presented in Fig. 6 for a 9×9 reconstruction with an acceleration factor of A=3 and N_C=4 receiver coils. The unfolding permutation, shift permutation, complex permutation and inverse Fourier transform operators are illustrated in Fig. 6A, B, C and D, respectively. As all three permutations simply rearrange the order of the data that they premultiply, they do not individually induce any covariance, i.e., $P_U P_U^T = P_S P_S^T = P_C P_C^T = I$, and in turn induce an identity correlation between voxels. As the inverse Fourier transform reconstruction operator, Ω, is orthogonal, $\Omega\Omega^T = 1/(p_x p_y/A)I$, there is no correlation induced by image reconstruction, as illustrated in Fig. 6F, but the variances are reduced by a factor of $1/(p_x p_y/A)I$, as shown in Fig. 6E. The SENSE unfolding operator, U, resembles the block diagonal matrix, as illustrated in Fig. 6G, where each block unfolds the N_C real and N_C imaginary image values from the N_C coils into A real and A imaginary image values corresponding to the A folds. The voxel measurements from each of the N_C coils are covariant by the choice of the coil covariance matrix, Ψ. Therefore, as each block along the diagonal of U represents a $2N_C$ to $2A$ mapping of image values, there is a resulting block diagonal covariance between the corresponding voxels from each of the A folds in Fig. 6H. Consequently, the correlation induced by U in Fig. 6I is also of a similar block diagonal form. This correlation is purely a byproduct of the operator U itself

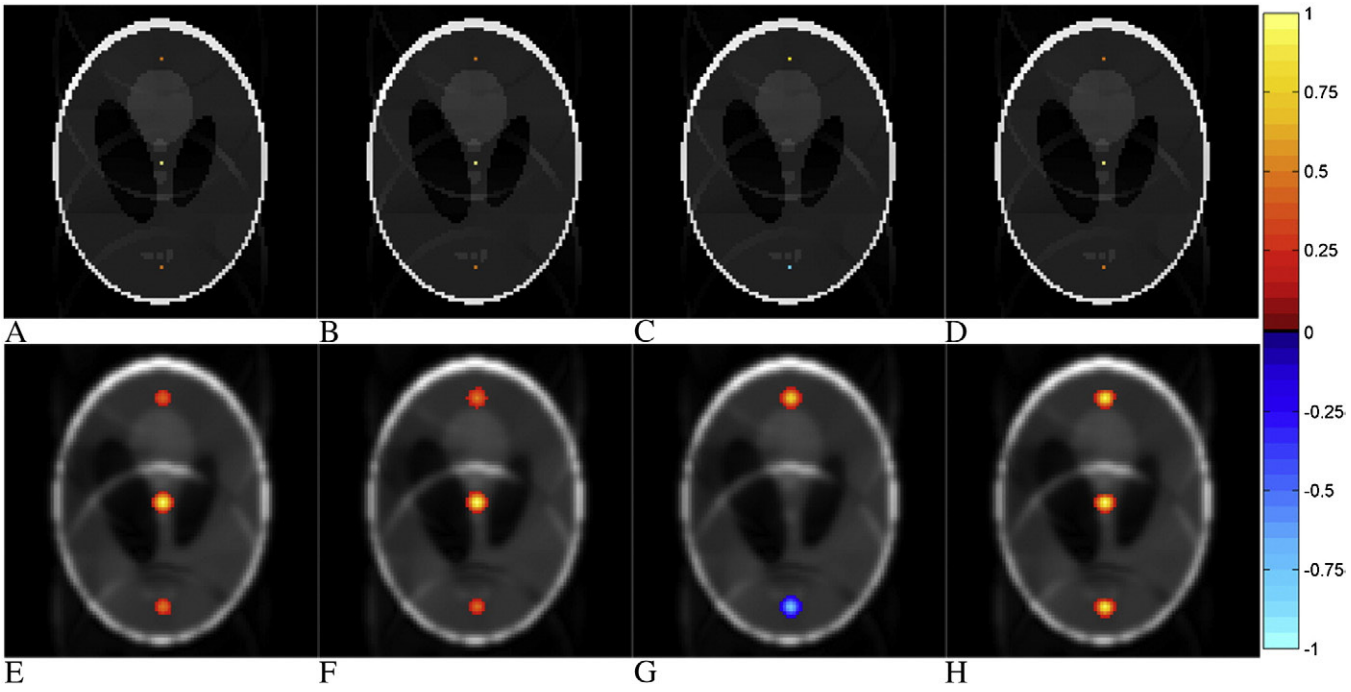

Fig. 7. Induced real, imaginary, real/imaginary and magnitude-squared voxel correlations about the center voxel by the SENSE operators with a threshold of 0.15. Smoothing was applied with a Gaussian kernel with an FWHM of three voxels to noiseless data, reduced in the PE direction for an acceleration factor of A=3. Correlations from operators with and without smoothing are presented with their respective magnitude underlay. (A) Real, (B) imaginary, (C) real/imaginary, (D) magnitude-squared, (E) smoothed real, (F) smoothed imaginary, (G) smoothed real/imaginary, (H) smoothed magnitude-squared.

and is therefore in place before any potentially correlated (or uncorrelated) data are introduced.

Upon closer inspection of the correlation from U, the real, imaginary and real/imaginary correlations between the center voxel and all other voxels in the reconstructed images are illustrated in Fig. 7A, B and C, respectively, with a threshold of 0.15, where the correlated voxels between folds are shown on the reconstructed magnitude image. Given that magnitude-only data have become the gold standard in image analysis, the magnitude-squared correlation about the center voxel is illustrated in Fig. 7D. Magnitude-squared data have been chosen because they are linear in nature and are asymptotically equivalent to magnitude-only data, which are not, and thus fit into the mathematical framework described throughout this manuscript. A mathematical derivation of the magnitude-squared covariance and correlation will not be presented in this manuscript, but can be found in Appendix B of Ref. [7]. While the correlations illustrated in Fig. 7 can be applied to any voxel in the reconstructed image, the center voxel is used throughout this manuscript for convenience.

It is evident in the real, imaginary and magnitude-squared correlation images in Fig. 7A, B and D that there is a positive correlation induced by the SENSE reconstruction operations between the center voxel and the corresponding center voxels of the upper and lower folds. It is important to note in Fig. 7C that, while there may be no real/imaginary correlation in the center voxel itself, the SENSE unfolding operation induces a real/imaginary correlation that is positive between the center voxel and the corresponding center voxels from the upper fold, and negative between the center voxel and the center voxel of the lower folds. The correlation induced between folds from the SENSE image reconstruction operators is further amplified if image smoothing is applied to the reconstructed images [7]. Illustrated in Fig. 7E–H, one can see that the correlated voxels from each fold maintain the same sign, but are now correlated clusters of voxels instead.

As these voxels are correlated purely by the image reconstruction operators, $\Sigma=OO^{T}$, with no contribution from the theoretical phantom data themselves, one would easily and mistakenly conclude that there is a correlation between voxels within the center, the anterior and the posterior regions of the brain in the center of each fold. This correlation could have serious implications in functional connectivity MRI studies. These correlations exemplify the importance of considering the effects of all operators utilized in image reconstruction, particularly when those operators involve image smoothing or image combining mappings such as SENSE.

4. Experimental application and analysis

To observe the statistical implications of the SENSE model on experimental data, two sets of data were acquired from an array of eight receiver coils in a 3.0-T General Electric Signa LX magnetic resonance imager. The first set of data was of a spherical agar phantom, while the second set was a series of nontask images of a human subject. Both data sets were composed of nine 2.5-mm-thick axial slices that are 96×96 in dimension for a 24-cm FOV, with the PE direction oriented as anterior to posterior (top–bottom in images). Acquired for a series of 510 TRs, the data sets had a repetition time (TR) of 1 s, an effective echo time of 42.8 ms, an effective echo spacing of 768 ms, a flip angle of 45° and an acquisition bandwidth of 125 kHz. The first 20 TRs were discarded to account for T_1 effects and because the echo time had been varied (in the human data), resulting in 490 TRs that were all acquired under the same conditions. All of the remaining 490 images from coils 1, 3, 5 and 7 were used in estimating both the sensitivity maps and the coil covariances, from N_C=4 equally spaced coils, to be used in image reconstruction. Subsampling was simulated for an acceleration factor of A=3 by deleting lines of k-space in each of the acquired coil images in the PE direction.

Both the spherical phantom data and the human subject data were acquired with a custom echo planar imaging (EPI) pulse sequence and reconstructed using locally developed image reconstruction software. The center line of k-space for each receiver coil was acquired with three navigator echoes in order to estimate the error in the center frequency and group delay offsets between the odd and even k-space lines [7]. As EPI techniques are susceptible to dynamic fluctuations in the homogeneities of the main magnetic field, the global, temporal phase structure was corrected in both data sets after unfolding to account for field shifts associated with gradient heating and radiofrequency phase variation [8].

Traditionally, the raw coil sensitivity maps would be derived by normalizing the surface coil sensitivities in each voxel by the corresponding body coil sensitivities [10]. As a body coil was not available from either of the scans, the raw coil sensitivity maps were thus normalized by dividing the surface coil sensitivities by an average of the coil sensitivities in each voxel. Alternatively, a square root of the sum of squares of the coil sensitivities in each voxel could be used [10,11]. However, little difference was observed between the root sum of squares sensitivity map and the simple average. As such, the simple average sensitivity maps were used in this study, as they provide both magnitude and phase images when the root sum of squares sensitivities do not have a phase. It is important to be able to reconstruct magnitude and phase images, as they allow the use of all of the data in determination of voxel activation from complex-valued time series [12,13].

4.1. Phantom data

To bridge the gap between the theoretical illustration in Section 3 and the application to the human subject data to follow, a spherical agar phantom was scanned. Unlike a human subject, the phantom is not prone to respiratory movement or physiological effects and thus provides a good

Table 1
Coil covariances estimated from real data assuming an identity voxel covariance

0.0863	0.0083	0.0112	0.0439	0.0013	0.0188	−0.0282	0.0149
0.0083	0.0149	0.0059	0.0184	−0.0153	0.0002	−0.0149	0.0046
0.0112	0.0059	0.0779	−0.0383	0.0186	0.0094	−0.0003	0.0403
0.0439	0.0184	−0.0383	0.1342	−0.0083	0.001	−0.0619	0.0135
0.0013	−0.0153	0.0186	−0.0083	0.0774	0.0075	0.0164	0.0296
0.0188	0.0002	0.0094	0.001	0.0075	0.0151	0.0051	0.0148
−0.0282	−0.0149	−0.0003	−0.0619	0.0164	0.0051	0.0928	−0.0379
0.0149	0.0046	0.0403	0.0135	0.0296	0.0148	−0.0379	0.1037

baseline for experimental observations. Coil sensitivity maps were estimated from the experimental time series of phantom images by dividing the surface coil sensitivities in each voxel within each coil by an average of the coil sensitivities in each voxel and then averaging over the time series. An analysis was performed on the statistical properties of reconstructed images by observing both the estimated correlation between voxels over the course of the time series after image reconstruction as well as the correlations induced by the reconstruction operators alone.

4.1.1. Estimated coil covariance

In order to perform the SENSE image reconstruction process on the experimental data set, the $2N_C \times 2N_C$ real-valued isomorphism representation of the complex coil-covariance matrix was evaluated from the observed aliased voxel values. Provided with a time series of N_{TR} complex-valued, aliased, k-space arrays of dimension $p_x \times p_y/A$, let V denote a $p_x p_y/A \times 2N_C \times N_{TR}$ real-valued array composed of the N_C real and N_C imaginary vectorized components of the image-space images from the N_C coils in each TR. From the three-dimensional array V, the mean can be taken in the third dimension to estimate the mean image $\overline{V}$. Thus, the coil covariance can be estimated as

$$\hat{\Psi}_{\text{coil}} = \frac{1}{N_{TR} * \text{rp}} \sum_{t=1}^{N_{TR}} (V_t - \overline{V})^{\text{T}} I_{\text{rp}}^{-1} (V_t - \overline{V}). \tag{23}$$

The estimated real-valued isomorphism representation of the $2N_C \times 2N_C$ complex coil covariance matrix, $\hat{\Psi}_{\text{coil}}$, in Eq. (23), from the time series of 490 TRs from N_C=4 receiver coils, is listed in Table 1. Upon observation, if the estimated coil covariance, $\hat{\Psi}_{\text{coil}}$, in Table 1 is partitioned into $N_C \times N_C$ real-valued quadrants as

$$\hat{\Psi}_{\text{coil}} = \begin{bmatrix} \Psi_1 & \Psi_2 \\ \Psi_3 & \Psi_4 \end{bmatrix},$$

it can be seen that $\Psi_3 = \Psi_2^{\text{T}}$ and $\Psi_1 \approx \Psi_4$. The fact that $\Psi_1 \approx \Psi_4$ reinforces the assumption made in generating the data in the theoretical illustration where $\Psi_R = \Psi_I$, based on the use of the complex-valued normal distribution of the Fourier coefficients. To accommodate the skew-symmetric coil covariance structure assumed by the SENSE model in Eq. (16), the estimated coil covariance is reordered into

$$\hat{\Psi}_{\text{SE}} = \begin{bmatrix} \Psi_1 & -\Psi_4 \\ \Psi_4 & \Psi_1 \end{bmatrix},$$

replacing Ψ_2 and Ψ_3 with $-\Psi_4$ and Ψ_4, respectively. This substitution is necessary because $\hat{\Psi}_{\text{coil}}$ is not skew-symmetric, and the skew-symmetric coil covariance assumed by the SENSE model in Eq. (16) does not have an explicitly defined real/imaginary covariance, but rather substitutes the imaginary covariance into the off-diagonal quadrants. The only way in which the skew-symmetric coil covariance in Eq. (16) could be equivalent to $\hat{\Psi}_{\text{coil}}$ would be if $\hat{\Psi}_{\text{coil}}$=0, which is not the case and would result in an unfolding operator filled with zeros.

To gain a better understanding of the covariance structure between coils, an average covariance was formed. This was done by taking the mean of the diagonals of each quadrant of $\hat{\Psi}_{\text{SE}}$. In an array of four coils, the main diagonal corresponds to the coil of interest, the second and fourth supra- and subdiagonals correspond to the neighboring coils, and the

Table 2
Averaged coil correlation estimated from data assuming an identity voxel covariance

1	0.0632	0.189	0.0632	0.0487	−0.0285	−0.013	−0.0285
0.0632	1	0.0632	0.189	−0.0285	0.0487	−0.0285	−0.013
0.189	0.0632	1	0.0632	−0.013	−0.0285	0.0487	−0.0285
0.0632	0.189	0.0632	1	−0.0285	−0.013	−0.0285	0.0487
0.0487	−0.0285	−0.013	−0.0285	1	0.0145	0.2155	0.0145
−0.0285	0.0487	−0.0285	−0.013	0.0145	1	0.0145	0.2155
−0.013	−0.0285	0.0487	−0.0285	0.2155	0.0145	1	0.0145
−0.0285	−0.013	−0.0285	0.0487	0.0145	0.2155	0.0145	1

third supra- and subdiagonals correspond to the opposing coil. This averaged covariance structure was then transformed into the correlation matrix in Table 2 by

$$\mathrm{corr}\left(\hat{\Psi}_{\mathrm{SE}}\right) = D_{\Psi}^{-1/2}\hat{\Psi}_{\mathrm{SE}}D_{\Psi}^{-1/2},$$

where D_{Ψ} is a diagonal matrix of the variances from the diagonal of $\hat{\Psi}_{\mathrm{SE}}$ and the superscript $-1/2$ denotes the reciprocal of the square root of D_{Ψ}. Upon closer inspection of the real component of coil correlation in Table 2, one can see that the correlation between the coils along the diagonal and their neighbors loosely follows a circular Markovian structure (as used in the theoretical illustration).

The 490 images of the spherical phantom data set were reconstructed using the SENSE reconstruction operators

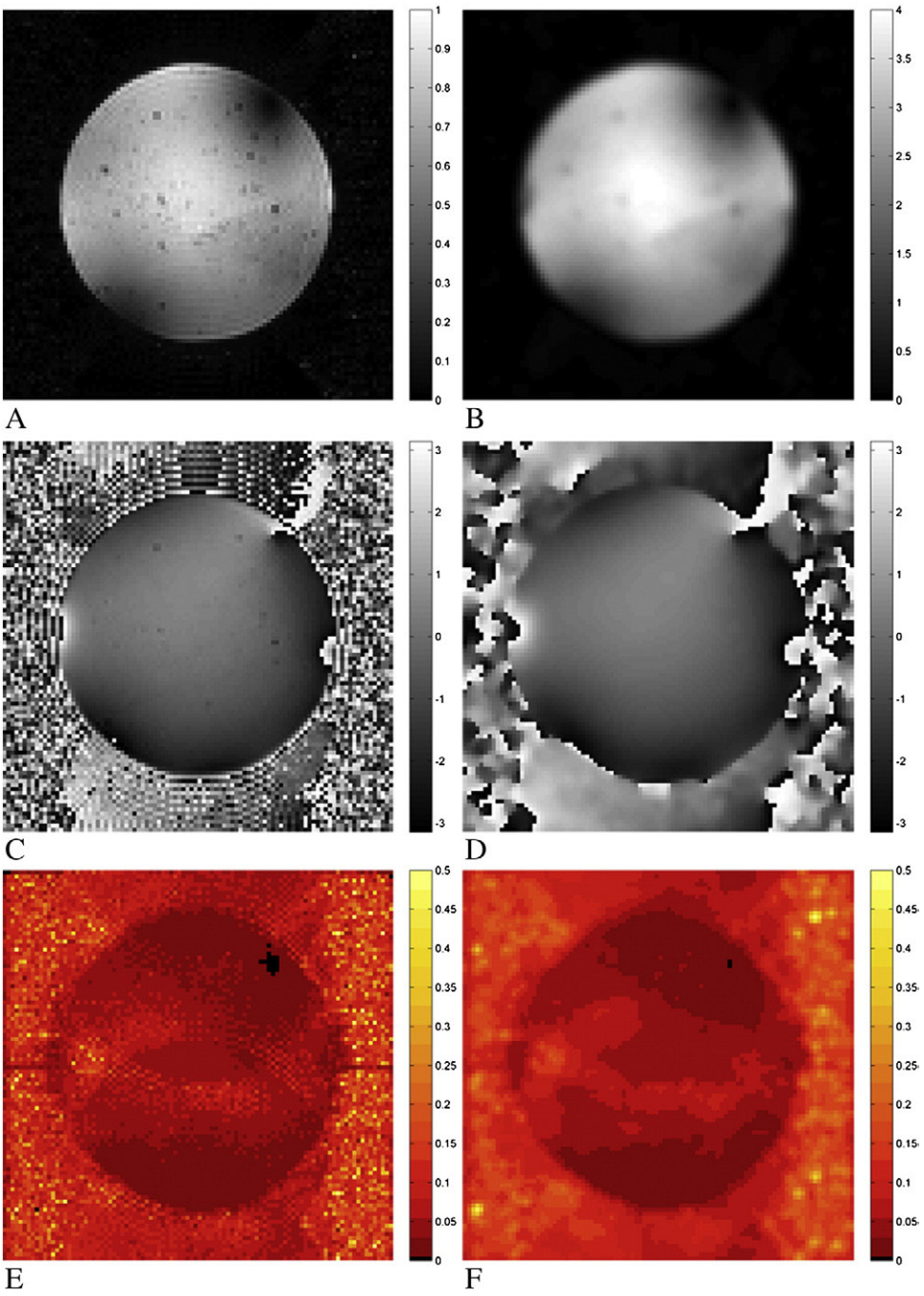

Fig. 8. SENSE mean magnitude, mean phase and standard deviation images from phantom data. Smoothing was applied with a Gaussian kernel with an FWHM of three voxels. (A) Unsmoothed magnitude, (B) smoothed magnitude, (C) unsmoothed phase, (D) smoothed phase, (E) unsmoothed standard deviation, (F) smoothed standard deviation.

assuming an identity voxel covariance structure in Eq. (19). Mean magnitude and phase images were constructed with an acceleration factor of A=3, as illustrated in Fig. 8A and C. While it is not immediately evident in the mean magnitude and phase images, the standard deviation in Fig. 8E shows signs of aliasing within the phantom. In both the phase and

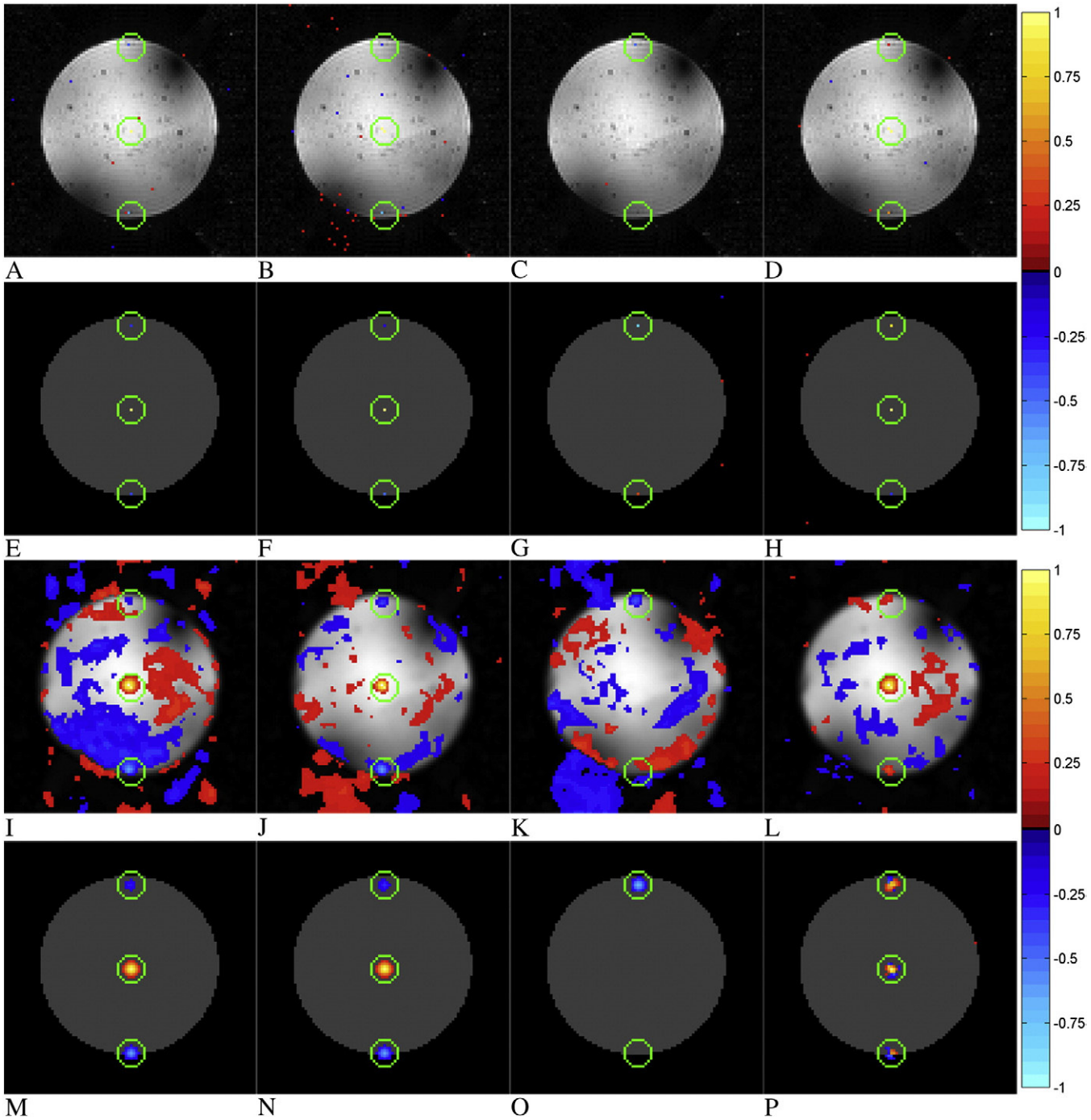

Fig. 9. Estimated correlations about the center voxel throughout the time series of 490 phantom images reconstructed via the SENSE image reconstruction operators and correlations induced by the SENSE image reconstruction operators. Correlations presented with a threshold of 0.15, where estimated correlations are presented with a magnitude underlay, while operator-induced correlations are presented on a theoretical circular phantom. (A) Real estimated correlation, (B) imaginary estimated correlation, (C) real/imaginary estimated correlation, (D) magnitude-squared estimated correlation, (E) real operator-induced correlation, (F) imaginary operator-induced correlation, (G) real/imaginary operator-induced correlation, (H) magnitude-squared operator-induced correlation, (I) real estimated correlation with smoothing, (J) imaginary estimated correlation with smoothing, (K) real/imaginary estimated correlation with smoothing, (L) magnitude-squared estimated correlation with smoothing, (M) real operator-induced correlation with smoothing, (N) imaginary operator-induced correlation with smoothing, (O) real/imaginary operator-induced correlation with smoothing, (P) magnitude-squared operator-induced correlation with smoothing.

standard deviation images in Fig. 8C and E, there appears to be some level of aliasing above and below the phantom. This aliasing outside of the phantom is a result of both Nyquist ghosting that has not been completely removed as well as the correlation induced between aliased voxels in the SENSE image reconstruction process.

To illustrate the effects of image smoothing, each reconstructed image in the time series of phantom data was smoothed using a Gaussian kernel with an FWHM of three voxels. As is expected with the implementation of a Gaussian-smoothing kernel, scaled to achieve a constant variance as outlined in Appendix A, the magnitude in Fig. 8B has been scaled up by a factor of 4.5, correspondent with the selection of the FWHM, as illustrated in Fig. 8B. It is of note in the smoothed standard deviation in Fig. 8F that while the variance within each voxel is unchanged by the implementation of the smoothing kernel, the covariance between voxels is increased. Upon observation of the unsmoothed and smoothed standard deviation images in Fig. 8E and F, respectively, the standard deviation within the phantom is considerably lower than that outside, with the exception of the regions in which the aliasing occurs in the center.

A two-part analysis was performed on the correlations between voxels after the time series was reconstructed using the SENSE model. First, images of the correlation over the time series were constructed between the center voxel and all other voxels in the image by reshaping the row of the overall correlation matrix corresponding to the center voxel. Second, correlation images were produced to illustrate the correlation induced by the image reconstruction operators alone. Presented in Fig. 9A–D, with a magnitude underlay, are the real, imaginary, real/imaginary and magnitude-squared correlations between the center voxel and all other voxels in the image over the course of the time series. By comparing Fig. 9A–D with the real, imaginary, real/imaginary and magnitude-squared operator-induced correlations in Fig. 9E–H, one can see that there is a negative real, a negative imaginary, a positive and negative real/imaginary, and a positive magnitude-squared correlation between the center voxel and the respective center voxel from the top and bottom folds. Fig. 9I–L illustrates the correlation estimated between the center voxel and all other voxels over the course of the time series with image smoothing, and Fig. 9M–P illustrates the correlations induced purely by the image reconstruction operators with image smoothing applied in image space. By comparing the real, imaginary, real/imaginary and magnitude-squared correlations estimated over the time series in Fig. 9I–L to the operator correlations in Fig. 9M–P, it is evident that there are clusters of voxels in the center of the center, upper and lower folds that are correlated to the center voxel. As the assumption was made that there was an identity covariance structure between voxels before image reconstruction, these correlations are therefore a byproduct of the SENSE unfolding process and would be misinterpreted if no steps were taken to account for operator-induced correlations.

4.2. Human subject data

Unlike a static spherical phantom, data acquired for a human subject are prone to respiratory movement and physiological effects. Coil sensitivity maps and coil covariances were estimated from the time series of human subject images. An analysis was performed on the statistical properties of reconstructed images by observing both the estimated correlation between voxels over the course of the time series after image reconstruction as well as the correlations induced by the reconstruction operators alone.

4.2.1. Estimated coil covariance

Following the same procedure used with the phantom data set, the $2N_C \times 2N_C$ real-valued isomorphism representation of the complex coil-covariance matrix was evaluated from the observed aliased voxel values using Eq. (23). This $2N_C \times 2N_C$ covariance was again partitioned into quadrants such that it could be reorganized to accommodate the skew-symmetric coil covariance assumed by the SENSE model. The 490 images in the time series were then individually reconstructed using the SENSE image reconstruction operators, with an acceleration factor of $A=3$, in conjunction with the estimated coil sensitivity profiles and the estimated coil covariance structure, both with and without image smoothing.

The mean magnitude and phase images, without and with smoothing, are illustrated in Fig. 10A–D. As expected, the effect of applying a Gaussian-smoothing kernel is an increase in the mean magnitude in each voxel. A Gaussian kernel with an FWHM of three voxels should result in an increase in the voxel mean by a factor of 4.5, which is not the case for the human subject data set. This is in part a result of the temporal off-resonance alignment of single-echo time-series correction scheme utilized to account for temporal variations in the magnetic field within the brain over the course of the time series [8]. While aliasing was evident in the phantom standard deviation images in Fig. 8E and F, it is not as apparent in the standard deviation images for the human subject data in Fig. 10E and F. In both the phase and standard deviation images, however, there still appears to be some level of aliasing above and below the brain because of both Nyquist ghosting that has not been completely removed and the correlation induced between aliased voxels via the SENSE image reconstruction process. As image smoothing induces a correlation between voxels and their neighbors, it is to be expected that the standard deviation within a voxel will remain unchanged if the smoothing kernel is scaled to maintain a constant variance in each voxel, while the covariance between voxels will be increased, as illustrated when comparing the standard deviation images without image smoothing in Fig. 10E to those with smoothing in Fig. 10F. As was noted in the phantom data set, both the unsmoothed and smoothed standard deviations, in Fig. 10E

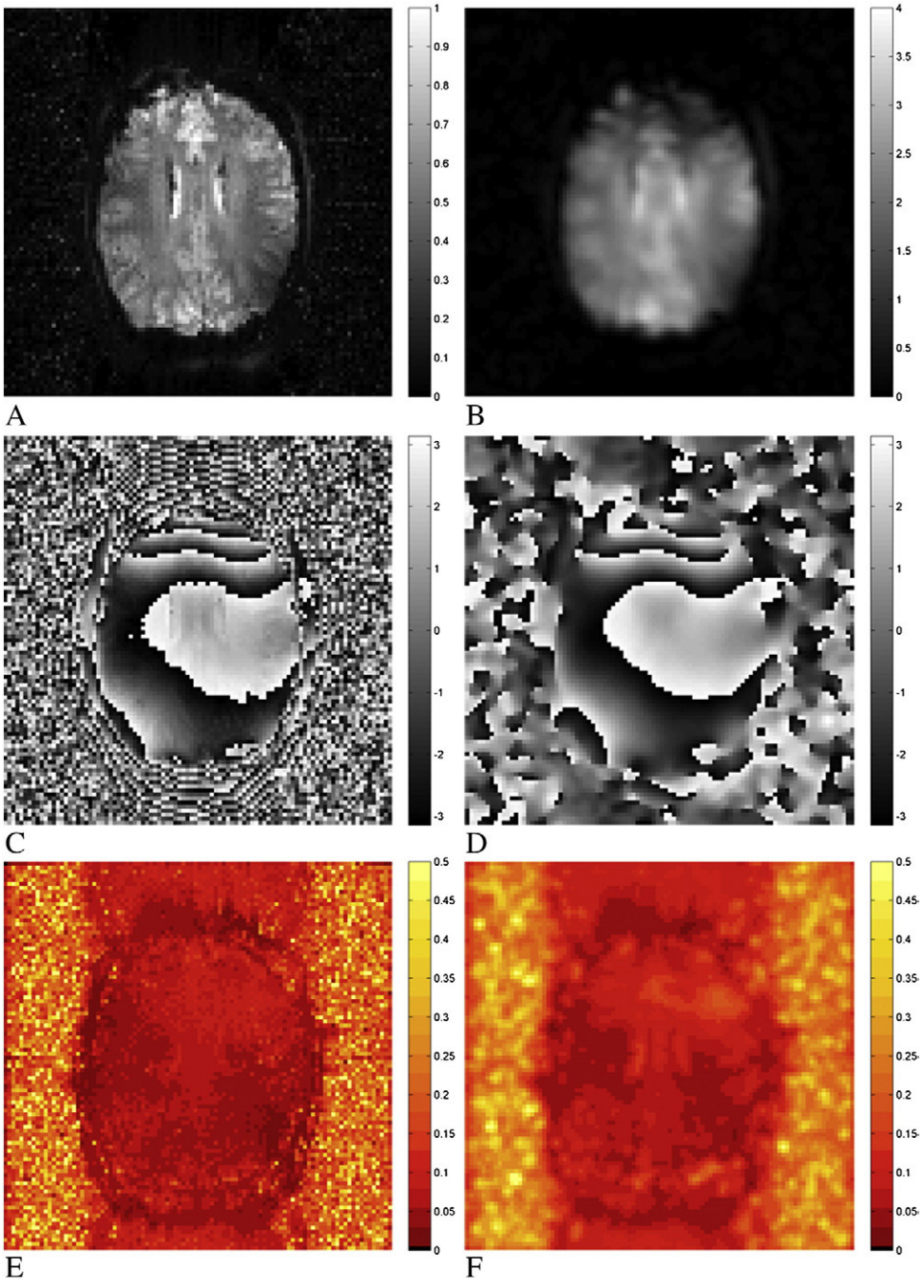

Fig. 10. SENSE mean magnitude, mean phase and standard deviation images from human subject data. Smoothing was applied with a Gaussian kernel with an FWHM of three voxels. (A) Unsmoothed magnitude, (B) smoothed magnitude, (C) unsmoothed phase, (D) smoothed phase, (E) unsmoothed standard deviation, (F) smoothed standard deviation.

and F, respectively, are lower within the subject to that outside the subject.

A similar two-part analysis was performed on the correlations in the human subject data set to those in the phantom data set, where the correlations estimated throughout the time series of human subject data between the center voxel and all other voxels in the full FOV reconstructed images are compared to the correlations induced by the SENSE image reconstruction operators alone. Illustrated in Fig. 11A–D, with a magnitude underlay, are the real, imaginary, real/imaginary and magnitude-squared correlations between the center voxel and all other voxels in the image over the course of the time series. In the real, imaginary and real/imaginary correlation images, there appears to be a ripple effect within the brain, which may be due to the relative quadrant in which the phase of the center voxel and other voxels reside. This ripple effect is a result of phase correlations resulting from physiological

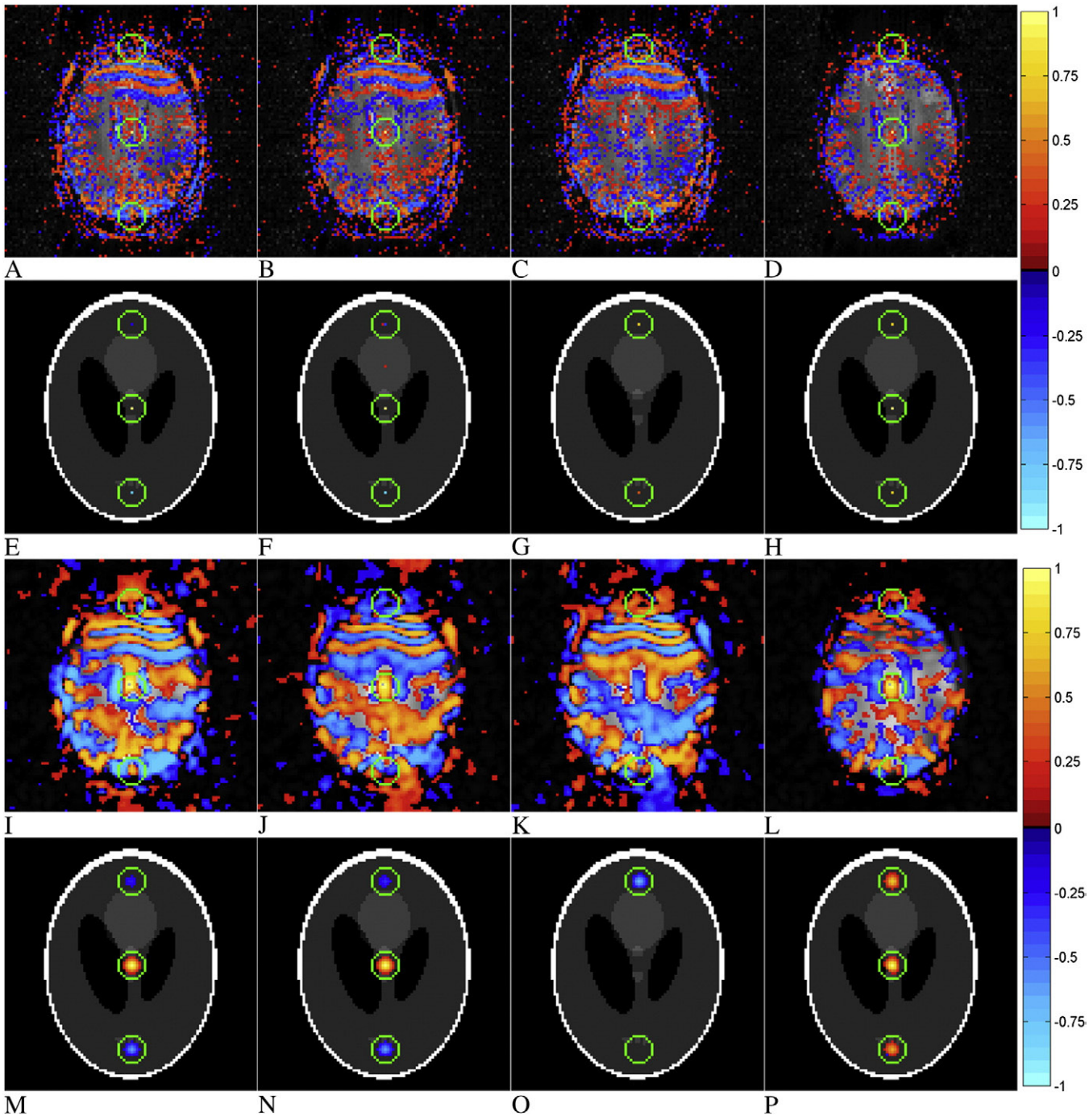

Fig. 11. Estimated correlations about the center voxel throughout the time series of 490 human subject images reconstructed via the SENSE image reconstruction operators and correlations induced by the SENSE image reconstruction operators. Correlations presented with a threshold of 0.15, where estimated correlations are presented with a magnitude underlay, while operator-induced correlations are presented on a theoretical circular phantom. (A) Real estimated correlation, (B) imaginary estimated correlation, (C) real/imaginary estimated correlation, (D) magnitude-squared estimated correlation, (E) real operator-induced correlation, (F) imaginary operator-induced correlation, (G) real/imaginary operator-induced correlation, (H) magnitude-squared operator-induced correlation, (I) real estimated correlation with smoothing, (J) imaginary estimated correlation with smoothing, (K) real/imaginary estimated correlation with smoothing, (L) magnitude-squared estimated correlation with smoothing, (M) real operator-induced correlation with smoothing, (N) imaginary operator-induced correlation with smoothing, (O) real/imaginary operator-induced correlation with smoothing, (P) magnitude-squared operator-induced correlation with smoothing.

effects within the human subject over the course of the time series. This explanation is supported by a lack of a similar effect in the magnitude-squared correlation.

The comparison between the correlations in Fig. 11A–D to those in Fig. 11E–H is more difficult to make than in the case of the phantom data set, as there appear to be many

voxels correlated with the center voxel in the human subject data set. In the event of image smoothing, in Fig. 11I–P, one can see that there is a positively correlated cluster of voxels about the center voxel in the real, imaginary and magnitude-squared correlation images. While there is no such correlated cluster of voxels in the center of the real/imaginary operator correlation in Fig. 11O, there appears to be a negative real/imaginary correlation in the center of the correlation estimated over the time series in Fig. 11K. It is again important to note that the SENSE model assumes an identity covariance structure between voxels before image reconstruction, and therefore any correlation estimated after the fact is a byproduct of the SENSE image reconstruction process and preprocessing operations.

5. Discussion

This work extends the mathematical framework outlined in Refs. [6,7] that allows image reconstruction operators to be expressed as matrices and thus used to determine the statistical effects that each operator induces on the mean, covariance and correlation of the data to be reconstructed. In this article, the mathematical framework of Ref. [7] has been adapted to incorporate data that have been subsampled and acquired from an array of multiple receiver coils. We have provided a framework for analyzing the SENSE model as an isomorphism, allowing an analysis to be performed on the unfolding operator that is applied to the acquired data. In representing the SENSE model in terms of a real-valued isomorphism, one can see that the model assumes a skew-symmetric covariance structure between coils as a result of the conjugate transpose utilized in the complex-valued weighted least squares estimation process. As this covariance is unlike that of real data, it was shown in the theoretical illustration of a 96×96 modified Shepp–Logan phantom that aliasing becomes apparent in both magnitude and phase images.

An investigation into the SENSE image reconstruction model for a 9×9 image showed that the three permutation matrices and inverse Fourier transform matrix are all orthogonal, producing either an identity matrix or a scaled identity matrix when multiplied by their respective transposes. As such, there is no correlation induced by the permutations or inverse Fourier transformation. The SENSE unfolding operation, however, is a block diagonal matrix that performs a mapping from the N_C real and N_C imaginary aliased voxel values from the N_C coils into A real and A imaginary unaliased voxel values corresponding to the A folds and is therefore not orthogonal. It was shown in the reconstruction of a 96×96 modified Shepp–Logan phantom that the SENSE model induces a correlation between each of the previously aliased voxels in each fold. This correlation between the A unaliased voxels becomes more severe when image smoothing is applied, resulting in correlated clusters of voxels instead.

As the SENSE model assumes an identity covariance structure between voxels before image reconstruction, any correlation observed between the previously aliased voxels is therefore altered by the unfolding process defined by the model. This was shown for both a spherical phantom and a human subject, acquired from a 3.0-T Signa LX magnetic resonance imager. The correlation estimated about the center voxel over the course of a time series of 490 acquisitions after image reconstruction using the SENSE model showed that there was a correlation between the center voxel and the corresponding center voxel from the upper and lower folds, similar to the correlations induced by the image reconstruction operators alone. These three regions correlated to the center voxel correspond to the three previously aliased voxels unaliased by the SENSE unfolding operation with an acceleration factor of A=3. Should the acceleration factor be increased, there would be an increase in the number of correlated regions that correspond to the number of previously aliased voxels defined by the acceleration factor A. An increase in the acceleration factor is only possible with an increase in the number of coils, such that the inversion in the least squares estimation in the SENSE model is possible. However, an increase in the number of coils similarly has an increase in the correlation between coils. As such, increasing the number of coils as well as the acceleration factor may provide an attractive decrease in the data acquisition time, but conversely results in an increase in correlation between both voxels and coils. As a means of accounting for this correlation, one could subtract the inherent local spatial correlation in each voxel as described in Ref. [14]; however, this may not be the most optimal method. The induced temporal correlation should be utilized in computing each voxel's level of activation. The induced spatial correlation should be utilized in a larger spatiotemporal model or perhaps in the proper threshold determination.

The isomorphism outlined in this article, however, is very computationally intensive. In order to reconstruct a 96×96 image, with real and imaginary data, from an array of N_C=4 receiver coils that gather subsampled data with an acceleration factor of A=3, the operator matrix O would be 24,576×73,728. For subsampled data from an array of N_C=8 receiver coils, gathering subsampled data with an acceleration factor of A=3, the operator matrix O would be 49,152×147,456. Thus, the number of elements within the operators scales with N_C^2. This framework can also be extended to reconstruct images in a time series with time series processing operators. However, if all spatial and temporal operators were combined into a single operator, the number of elements would scale by the square of the number of images in the time series. Therefore, the use of sparse matrices and parallel matrix multiplication techniques, such as the parallel universal matrix multiplication algorithm [15] and the scalable parallel universal matrix multiplication algorithm [16], would be encouraged.

Despite the high dependence on computational resources, the framework outlined in this article provides an invaluable tool for analyzing the exact correlation induced by operators used in parallel image reconstruction models such as SENSE. The results indicate that operators that perform a mapping of data from multiple receiver coils to multiple folds when unaliasing an aliased image induce a correlation between aliased voxels. Representing the image reconstruction operators as a real-valued isomorphism allows one to observe the correlation induced by all operators in each voxel of the reconstructed image. As this induced correlation is purely a result of the operators involved in reconstruction and not of any biological origin, this framework can have strong implications in functional connectivity studies. Therefore, the framework outlined in this article could allow one to account for the effects each reconstruction operator has on the data in subsequent analysis.

Appendix A. Statistical effects of smoothing

As is common practice in fMRI, a Gaussian-smoothing kernel can be used to smooth the reconstructed images. It is important, however, to understand the effects such an operation has on the statistical properties of the data. Consider a Gaussian kernel in the center of a $2n\times 2m$ FOV with a mean of zero and a variance of σ^2

$$G(p_x,p_y) = \frac{1}{2\pi\sigma^2} e^{-\frac{\left(p_x^2 + p_y^2\right)}{2\sigma^2}}. \quad (A1)$$

It can be shown that the relationship between the FWHM, F, and variance of a Gaussian distribution is

$$F^2 = 2\sqrt{2ln(2)\sigma^2},$$

and thus the Gaussian kernel in Eq. (A1) can be represented in terms of the FWHM as

$$G(p_x,p_y) = \frac{4ln(2)}{\pi F^2} e^{-\frac{4ln(2)\left(p_x^2 + p_y^2\right)}{\pi F^2}}. \quad (A2)$$

If one were to apply the kernel in Eq. (A2) to each voxel $j=(p_x,p_y)$ in a Cartesian grid where $p_x=[-m{:}m]$ and $p_y=[-n{:}n]$, with an expected value of v_j and a variance of α^2, within the reconstructed image, it would result in no change in the voxel mean,

$$E\left(\sum g_j \times v_j\right) = \sum g_j \times v_j = v_j,$$

and a change in the voxel variance as

$$var\left(\sum g_j \times v_j\right) = \sum g_j^2 \times var(v_j) = \sum g_j^2 \alpha^2.$$

In order to prevent a change in variance, it is necessary to divide all elements of the Gaussian kernel in Eq. (A2) by the square root of the sum of the squares of all elements within the kernel. This results in a scaled mean

$$E\left(\sum \frac{g_j}{\sqrt{\sum g_j^2}} \times v_j\right) = \sum \frac{g_j}{\sqrt{\sum g_j^2}} \times v_j = \frac{1}{\sqrt{\sum g_j^2}} v_j$$

and the original variance

$$var\left(\sum \left(\frac{g_j}{\sqrt{\sum g_j^2}}\right)^2 \times v_j\right) = \sum \frac{g_j^2}{\sum g_j^2} \times var(v_j) = \alpha^2.$$

Therefore, the application of a Gaussian-smoothing kernel designed to leave the voxel variance unchanged has the effect of scaling the mean value within a voxel by a factor of

$$R = \frac{1}{\sqrt{\sum g_j^2}}.$$

This scaling factor R is directly related to the square of the FWHM, F, as

$$\begin{aligned} R &= \frac{1}{\sqrt{\sum g_j^2}} \\ &= \left[\sum_{p_x=-m}^{m}\sum_{p_y=-n}^{n}\left(\frac{4ln(2)}{\pi F^2} e^{-\frac{4ln(2)\left(p_x^2 + p_y^2\right)}{\pi F^2}}\right)^2\right]^{-1/2} \\ &= \frac{\pi F^2}{4ln(2)}\left[\sum_{p_x=-m}^{m}\sum_{p_y=-n}^{n} e^{-\frac{8ln(2)\left(p_x^2 + p_y^2\right)}{\pi F^2}}\right]^{-1/2}, \end{aligned}$$

and through the linear relationship between the FWHM and the kernel variance, R can be shown to be linearly related to the standard deviation of the kernel, σ.

References

[1] Lauterbur PC. Image formation by induced local interactions: examples employing nuclear magnetic resonance. Nature 1973;242:190–1.

[2] Haacke EM, Brown R, Thompson M, Venkatesan R. Magnetic resonance imaging: physical principles and sequence design. New York (NY): John Wiley and Sons; 1999.

[3] Hyde JS, Jesmanowicz A, Froncisz W, Kneeland JB, Grist TM, Campagna NF. Parallel image acquisition from noninteracting local coils. J Magn Reson 1986;70:512–7.

[4] Pruessmann KP, Weiger M, Scheidegger MB, Boesiger P. SENSE: sensitivity encoding for fast MRI. Magn Reson Med 1999;42:952–62.

[5] Blaimer M, Breuer F, Muller M, Heidemann RM, Griswold MA, Jakob PM. SMASH, SENSE, PILS, GRAPPA: how to choose the optimal method. Topics Magn Reson Imaging 2004;15:223–36.

[6] Rowe DB, Nencka AS, Hoffmann RG. Signal and noise of Fourier reconstructed fMRI data. J Neurosci Methods 2007;159:361–9.

[7] Nencka AS, Hahn AD, Rowe DB. A Mathematical Model for Understanding Statistical Effects of *k*-space (AMMUST-k) preprocessing on observed voxel measurements in fcMRI and fMRI. J Neurosci Methods 2009;181:268–82.

[8] Hahn AD, Nencka AS, Rowe DB. Improving robustness and reliability of phase-sensitive fMRI analysis using Temporal Off-resonance

Alignment of Single-echo Timeseries (TOAST). Neuroimage 2009;44: 742–52.
[9] Wooding RA. The multivariate distribution of complex normal variables. Biometrika 1956;43:212–5.
[10] Larkman DJ, Nunes RG. Parallel magnetic resonance imaging. Phys Med Biol 2007;52:15–55.
[11] Ying L, Liu B, Steckner MC, Wu G, Wu M, Li SJ. A statistical approach to SENSE regularization with arbitrary *k*-space trajectories. Magn Reson Med 2008;60:414–21.
[12] Rowe DB, Logan BR. A complex way to compute fMRI activation. Neuroimage 2004;23:1078–92.
[13] Rowe DB. Modeling both the magnitude and phase of complex-valued fMRI data. Neuroimage 2005;25(4):1310–24.
[14] Deshpande G, LaConte S, Peltier S, Hu X. Integrated local correlation: a new measure of local coherence in fMRI data. Hum Brain Mapp 2009;30:12–23.
[15] Choi J, Dongarra J, Walker DW. PUMMA: Parallel Universal Matrix Multiplication Algorithm on distributed memory concurrent computers. Concurr Pract Exp 1994;6:543–70.
[16] van de Geijn R, Watts J. SUMMA: Scalable Parallel Universal Matrix Multiplication Algorithm. LAPACK working note 99, technical report CS-95-286. University of Tennessee; 1995.